

Probing quantum-coherent dynamics with free electrons

H. B. Crispin* and N. Talebi†
*Institute for Experimental and Applied Physics,
Christian Albrechts University,
Leibnizstrasse 19, 24118 Kiel, Germany*

Recent advances in time-resolved cathodoluminescence have enabled ultrafast studies of single emitters in quantum materials with femtosecond temporal resolution. Here, we develop a quantum theory modeling the dynamics of free electrons interacting with quantum emitters in arbitrary initial states. Our analysis reveals that a free electron can induce transient coherent oscillations in the populations when the system is initially prepared in a coherent superposition of its states. Moreover, the electron energy spectrum exhibits a clear signature of the quantum coherence and sensitivity to the transition frequency of the emitter. These coherence effects manifest themselves as oscillations in the zero-loss peak of the spectral energy-loss probability. Our findings pave the way for characterization of quantum-coherent dynamics of individual quantum emitters by electron-probes.

Free electrons are powerful tools for characterizing and imaging material excitations at the nanoscale [1, 2]. Spectroscopic techniques such as cathodoluminescence (CL) and electron-energy-loss spectroscopy (EELS) can probe optical transitions of defect states with high spatial resolution [3]. EELS also provides access to the projected local density of photonic states [4]. However, these measurements have not demonstrated sensitivity to the quantum coherence, i.e., coherent superposition of energy states. Solid-state defects act as quantum emitters and offer novel functionalities that arise from their quantum-coherent properties [5], making them central to modern quantum technologies [6–8]. Therefore, characterization of the coherence dynamics is of fundamental importance for free electron-based spectroscopies.

Several theoretical schemes have shown that shaped electron wavefunctions can probe the atomic coherence [9–14]. Therefore, the off-diagonal density-matrix elements of the system are accessible at a given time. However, in order to probe the emitter dynamics, repeated measurements must ensure that the target of interest, e.g., a defect structure, is not altered or damaged during acquisition. This poses a challenge in free-electron-matter interactions [15]. More importantly, there is considerable interest in resolving the quantum dynamics in materials [15–18]. Quantum systems evolve on ultrashort timescales due to strong interactions under ambient conditions [17, 18]. For example, defect centers in novel two-dimensional materials such as hBN exhibit strong coupling to phonons. In such cases, the radiative decay and dephasing time of the quantum emitters is of the order of hundreds of femtoseconds [17]. Furthermore, recent time-resolved techniques [19] demonstrate the ability to probe ultrafast quantum-coherent processes in materials, inspiring studies of the dynamics of single emitters in their natural environment [17]. This motivates a general theoretical description for the free-electron-emitter interactions.

In this work, we develop a fully quantum, time-dependent theory for the coherent interaction between a free electron and quantum emitters in arbitrary initial states. The emitter is modeled as a two-level system, whose transition dipole moment couples to the Coulomb field of a moving Gaussian electron wavepacket. For various initial electron energies, we find that transient coherent oscillations can be induced in the populations when the system is prepared in an initial coherent superposition. In addition, we show that the electron energy spectrum is sensitive to the initial coherence and the transition frequency of the quantum emitter. These coherent effects appear as temporal oscillations centered on the zero-loss peak of the EELS probabilities. Finally, we discuss the dependence of the EELS spectra on the relative phase of the constituents of the superposition, revealing the ability of free electrons to probe the quantum-coherent dynamics.

I. THEORETICAL MODEL

We consider the interaction between the emitter and the free electron in the configuration shown in Fig. 1(a). We assume the electron wavepacket propagates along the z -axis in the $x - z$ plane with velocity v_0 . The quantum emitter, modeled as a two-level system with transition frequency ω_0 , is stationary at the origin. In this setup, the coherent interaction between the free electron and the emitter is given by the Hamiltonian [10]

$$H = H_{\text{qe}} + H_{\text{el}} + (\mathbf{d}_{eg}S^+ + \mathbf{d}_{eg}^*S^-) \cdot \vec{E}(r_{\perp}, 0, z). \quad (1)$$

Here, $H_{\text{qe}} = \hbar\omega_0\sigma_z/2$ and $H_{\text{el}} = -i\hbar v_0\partial_z$ are the free Hamiltonians of the quantum emitter and the propagating electron, respectively. The third term describes the interaction of the electron with the transition dipole moment $\mathbf{d}_{eg} = \mathbf{d}_x\hat{e}_x + \mathbf{d}_y\hat{e}_y + \mathbf{d}_z\hat{e}_z$ of the two-level system via its Coulomb field [20],

$$\vec{E}(r_{\perp}, 0, z) = \frac{-e\gamma}{4\pi\epsilon_0} \frac{(z\hat{e}_z + r_{\perp}\hat{e}_x)}{(\gamma^2 z^2 + r_{\perp}^2)^{3/2}}, \quad (2)$$

* Contact author: crispin@physik.uni-kiel.de

† Contact author: talebi@physik.uni-kiel.de

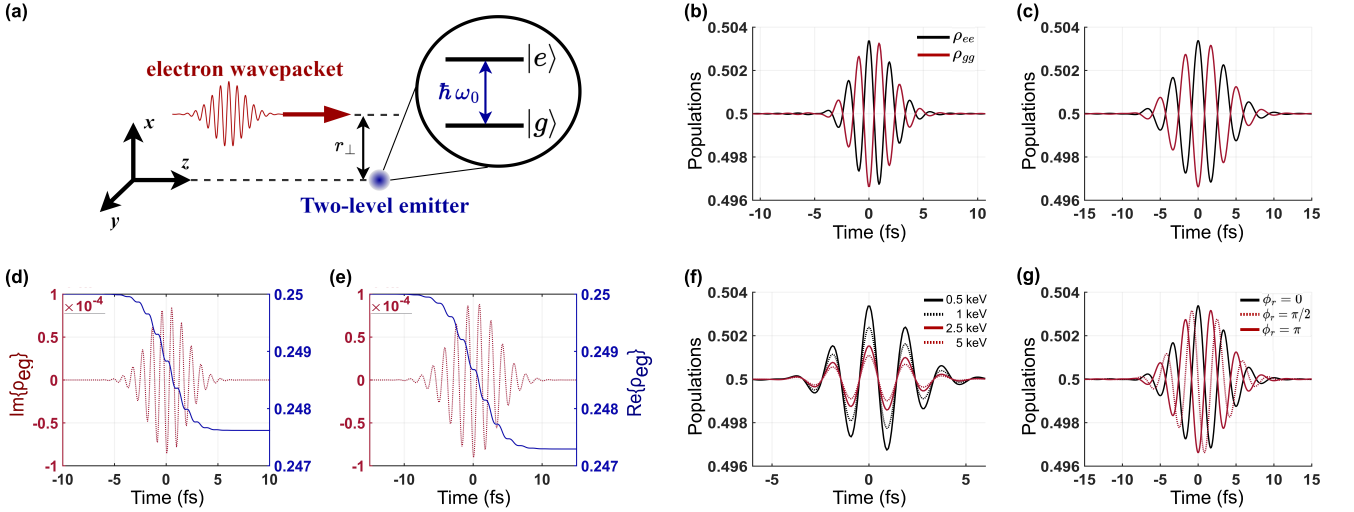


FIG. 1. (a) Schematic of the interaction between a two-level emitter and an electron wave packet. (b)–(e) Population (b),(c) and coherence (d),(e) dynamics for a 0.5 keV electron with impact parameter $r_\perp = 2$ nm. The emitter has $\mathbf{d}_x = \mathbf{d}_z = 30$ Debye and transition wavelengths of 560 nm in (b),(d) and 1000 nm in (c),(e); the initial state is $(|g\rangle + |e\rangle)/\sqrt{2}$. (f) Effect of increasing electron energy on the population dynamics for a 560 nm transition. (g) Effect of initial coherence on the population dynamics for a 1000 nm transition.

where $\gamma = 1/\sqrt{1 - v_0^2/c^2}$ is the Lorentz factor, ϵ_0 is the free space permittivity, and r_\perp is the impact parameter that represents the distance between the center of the moving electron wavepacket and the two-level emitter.

In obtaining the Hamiltonian (1), we employed the non-recoil approximation for the free electron. This approximation is justified when the initial electron energy E_0 is much greater than the transition energy $\hbar\omega_0$. We further assume that the interaction timescales involved are typically much shorter than the decoherence and dephasing times. We therefore neglect these effects in the present treatment.

To describe the dynamics of the total system including the free electron and the quantum emitter, it is helpful to move to the interaction picture $H_I(t) = U(H - H_0)U^\dagger$ with respect to the unitary transformation $U = \exp\{iH_0t/\hbar\}$, where $H_0 = H_{qe} + H_{el}$. The formal solution is

$$|\psi(t)\rangle = \mathcal{T}e^{-\frac{i}{\hbar} \int_{-\infty}^t H_I(t_1) dt_1} |\psi_{in}\rangle, \quad (3)$$

where \mathcal{T} denotes time ordering and $|\psi_{in}\rangle = |\psi_{qe}\rangle |\psi_{el}\rangle$ is the initial state. We consider the quantum state of the two-level emitter to be in a general coherent superposition $|\psi_{qe}\rangle = a|g\rangle + b e^{-i\phi_r} |e\rangle$ with ϕ_r being the relative phase. The initial free-electron state is a Gaussian wavepacket in the position basis,

$$|\psi_{el}\rangle = (2\pi\sigma_z^2)^{-1/4} \int dz e^{-\frac{z^2}{4\sigma_z^2} + ik_0 z} |z\rangle, \quad (4)$$

where $k_0 = E_0 v_0 / \hbar c^2$ for an electron of initial energy E_0 and spatial width σ_z .

Using the Magnus expansion [21], the joint free electron-emitter state, upto a normalization factor, can

be written in a compact form

$$|\psi(t)\rangle = \int dz e^{-\frac{z^2}{4\sigma_z^2} + ik_0 z} [c_g(z, t) |g\rangle + c_e(z, t) |e\rangle] |z\rangle, \quad (5)$$

with probability amplitudes,

$$\begin{aligned} c_g(z, t) &= [a \cos |g(z, t)| - i b e^{-i(\phi_r + \phi_g(z, t))} \sin |g(z, t)|], \\ c_e(z, t) &= [b e^{-i\phi_r} \cos |g(z, t)| - i a e^{i\phi_g(z, t)} \sin |g(z, t)|]. \end{aligned} \quad (6)$$

The expressions for the amplitudes $c_g(z, t)$ and $c_e(z, t)$ clearly show a relative phase dependence. In deriving (5), the higher-order terms in the Magnus expansion have been neglected, which is justified due to the weak coupling, $|g(z, t)| \ll 1$. In contrast to previous studies [10, 11], the coherent interaction is now governed by a complex, *time-dependent* coupling strength $g(z, t) = |g(z, t)| e^{i\phi_g(z, t)}$, where $\phi_g(z, t)$ is the phase [see Supplementary sections for the full derivation].

II. RESULTS AND DISCUSSION

A. Dynamics of the quantum emitter

We first consider the evolution of the two-level emitter, which can be obtained from the reduced density matrix $\rho_{qe}(t) = \text{Tr}_{el}\{\rho(t)\}$ with $\rho(t) = |\psi(t)\rangle \langle \psi(t)|$. Figs. 1(b) and 1(c) depict the population dynamics for quantum emitters whose transition frequencies lie in the optical ($\hbar\omega_0 \simeq 2.2$ eV) and the near-infrared region ($\hbar\omega_0 \simeq 1.2$ eV), respectively. The corresponding evolution of the coherences are displayed in Figs. 1(d) and 1(e). The free electron induces *Rabi-like* transient coherent oscillations in the populations and coherences when the electron wavepacket duration $\sigma_t = \sigma_z/v_0$ is comparable to or

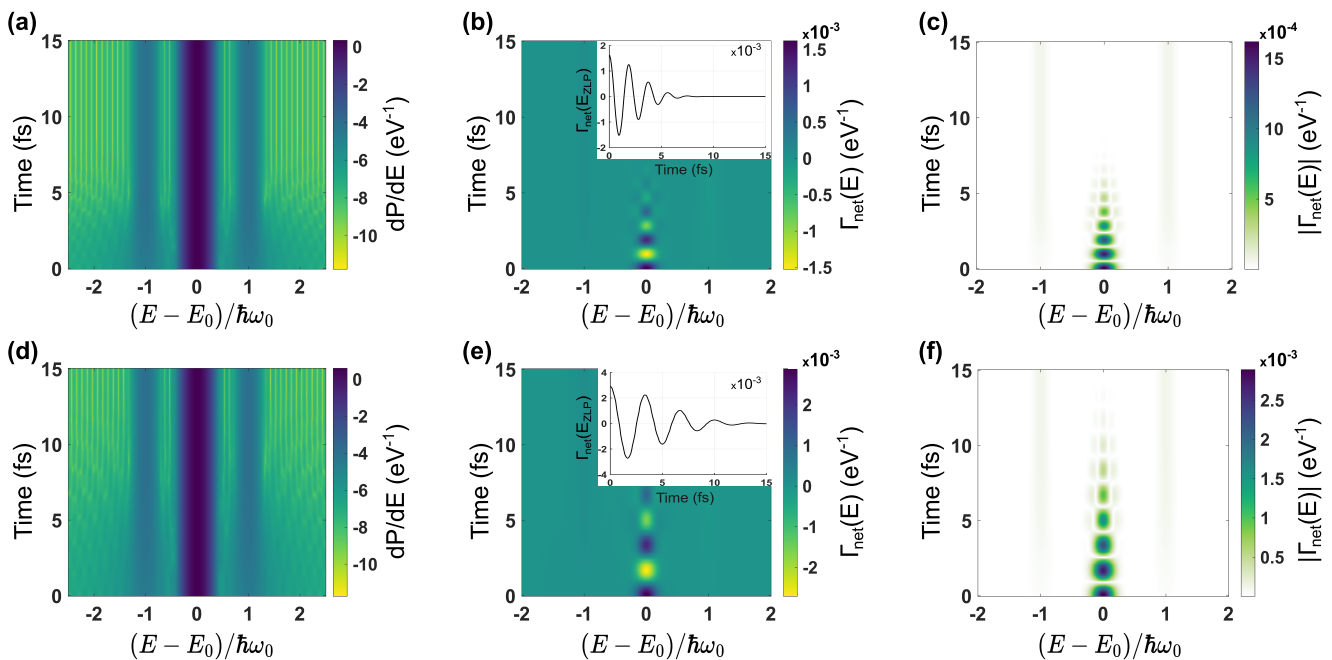


FIG. 2. (a),(d) Time-evolution of the EELS probability dP/dE for an electron with kinetic energy $\simeq 115$ keV ($v_0 = 0.578c$) for $t \geq 0$ and impact parameter $r_\perp = 2$ nm. The two-level emitter parameters in (a) and (d) are the same as in Fig. 1(b) and Fig. 1(c), respectively. (b),(e) Corresponding EELS probability differences $\Gamma_{net}(E)$ and its absolute value $|\Gamma_{net}(E)|$, showing the coherent oscillations in the zero-loss peak.

larger than the optical period $T = 2\pi/\omega_0$. The temporal envelope of these oscillations varies as a Gaussian $\sim e^{-t^2/\sigma_t^2}$. As a result, in comparison to optical transitions, one can see that the coherence effects occur over comparatively longer timescales for quantum emitters with infrared transitions [compare Fig. 1(b) and 1(c)]. We emphasize that the observed oscillatory features are prominent for coherent excitations by low energy electrons [Fig. 1(b)-(c) and 1(f)]. In comparison, the dynamics are difficult to be observed for fast electrons $E > 30$ keV. The effect of varying initial electron energies on the populations is shown in Fig. 1(f). For increasing electron velocities, we find that the coherent oscillations are suppressed. Nevertheless, the temporal features are still visible even for energies of a few keVs. More importantly, the population dynamics are sensitive to the relative phase ϕ_r of the initial superposition state. This dependence is illustrated in Fig. 1(g) for an equally weighted coherent superposition $|\psi_{in}\rangle = (|g\rangle + e^{-i\phi_r}|e\rangle)/\sqrt{2}$. A relative phase change from $\phi_r = 0$ to $\phi_r = \pi$ acts as a control parameter over the oscillations induced by the electron wavepacket. Therefore, it is interesting to investigate the electron energy spectrum for a signature of the quantum coherence of the two-level emitter.

B. EELS dynamics

To explore the coherence effects in the spectral electron energy loss probability, we compute the reduced density matrix of the free electron $\rho_{el}(t) = \text{Tr}_{qe}\{\rho(t)\}$. The diagonal elements in k -space provide information about the

EELS,

$$\frac{dP}{dE} = \langle k(E) | \rho_{el}(t) | k(E) \rangle = \frac{1}{\hbar v_0} \sum_{i=g,e} |\psi_i(k(E), t)|^2, \quad (7)$$

where $\psi_i(k(E), t) = N^{-1} \int dz e^{-z^2/4\sigma_z^2} e^{-ikz} c_i(z, t)$, $N = \sqrt{2\pi} (2\pi\sigma_z)^{1/4}$ is a multiplicative factor, and $k(E) = (E - E_0)/\hbar v_0$. Notably, the spectrum (7) is time-dependent and can be viewed as a time-resolved electron energy-loss spectrum. The terms ψ_g and ψ_e in Eq. (7) can be understood as the spectral probability amplitudes associated with the electron gaining and losing energy due to the interaction with the two-level emitter, respectively. The sum of the absolute square of these individual amplitudes gives the EELS probabilities of electron energy-loss $|\psi_e|^2$ and gain $|\psi_g|^2$. In the postinteraction EELS ($t \rightarrow \infty$), the quantum coherence information is lost for excitation by unshaped electrons [10]. However, the dynamics of the electron energy spectra reveals novel coherent properties.

We are interested in times $t > 0$ for which the electron wavepacket has crossed the two-level emitter. The spectral energy-loss probability for transition energies $\hbar\omega_0 \simeq 2.2$ eV and $\hbar\omega_0 \simeq 1.2$ eV can be seen in Figs. 2(a) and 2(d), respectively for $t \geq 0$. The electron energy gain $E = E_0 + \hbar\omega_0$ and loss peaks $E = E_0 - \hbar\omega_0$ are clearly visible in the spectra along with the prominent zero-loss peak $E = E_0$. We note that the probabilities associated with electron energy loss $|\psi_e|^2$ and gain $|\psi_g|^2$ depend on the relative phase ϕ_r [from Eq. (6) and (7)].

To clearly see the signature of quantum coherence in the EELS dynamics, we consider the probability difference

$$\Gamma_{net}(E) = \frac{1}{\hbar v_0} (|\psi_e(E)|^2 - |\psi_g(E)|^2), \quad (8)$$

where the time-dependence is implied. A remarkable feature is the coherent oscillations in the zero-loss peak [Figs. 2(b) and 2(e)], signifying the dynamics of the energy exchange between the electron wavepacket and the emitter. The minimum and maximum probabilities at a given time correspond to the net energy gained or lost by the free electron to the quantum emitter. The zeroes in the spectra [Figs. 2(b) and 2(e)] imply a net zero energy exchange, i.e., they denote times for which the emitter returns to the same initial state $|\psi_{in}\rangle$. A contour of the absolute values $|\Gamma_{net}(E)|$ clearly depicts the timescales for which the induced coherence effects survive [Figs. 2(c) and 2(f)], which agrees well with the corresponding results in Fig. 1(b)-(c). For an initial electron velocity $v_0 = 0.578c$ ($E \simeq 115\text{keV}$), the distance traversed by the electron after crossing the emitter for times $t \sim 4 - 6$ fs is comparable to or greater than the wavelength of the transitions considered. The induced coherence effects can therefore play a significant role for collective excitations of nearby quantum emitters. Interestingly, the period of the oscillations observed in the zero-loss peak [Fig. 2(b) and (e)] is determined by the transition frequency ω_0 of the quantum emitter being probed. In addition, the resulting dynamics is sensitive to the quantum coherence [Fig. 3]. The relative phase ϕ_r now acts as a tunable parameter to control the temporal features in the EELS spectra [Fig. 3(a)-(d)]. For shorter impact parameters, the probabilities oscillate with larger amplitudes [compare Fig. 3(a) and 3(b); 3(c) and 3(d)].

To intuitively understand these results, it is useful to express $g(z, t)$ in the frequency domain, $g(z, t) = \int d\omega \tilde{g}(\omega, t) e^{-i\omega \tilde{z}/v_0}$, where $\tilde{z} = z + v_0 t$. The coupling parameter $\tilde{g}(\omega, t)$ can be written as a sum of two parts,

$$\tilde{g}(\omega, t) = [\delta(\omega - \omega_0) g_q(\omega_0) + g_c(\omega)] e^{i\omega_0 t}, \quad (9)$$

a constant term and an exponential oscillatory part weighted by functions $g_q(\omega_0)$ and $g_c(\omega)$, respectively [see Supplementary sections for derivations and explicit forms]. It is clear that the Dirac delta contribution leads to exact energy translations $b(\omega_0)|E\rangle = |E - \hbar\omega_0\rangle$ and $b^\dagger(\omega_0)|E\rangle = |E + \hbar\omega_0\rangle$, where $b(\omega_0) = e^{-i\omega_0 z/v_0}$ can be identified as the electron momentum ladder operator $b(\omega_0)|E\rangle = |E - \hbar\omega_0\rangle$. Therefore, the electron can gain or lose energy $\hbar\omega_0$ due to the interaction with the two-level emitter [10]. A novel feature is the transient oscillatory component, which leads to intriguing effects in the dynamics of the EELS spectrum and the quantum emitter discussed here. In the long-time limit $t \rightarrow \infty$, the dynamical coupling reduces to the standard interaction constant g [9–11] (see Supplementary sections for detailed discussion).

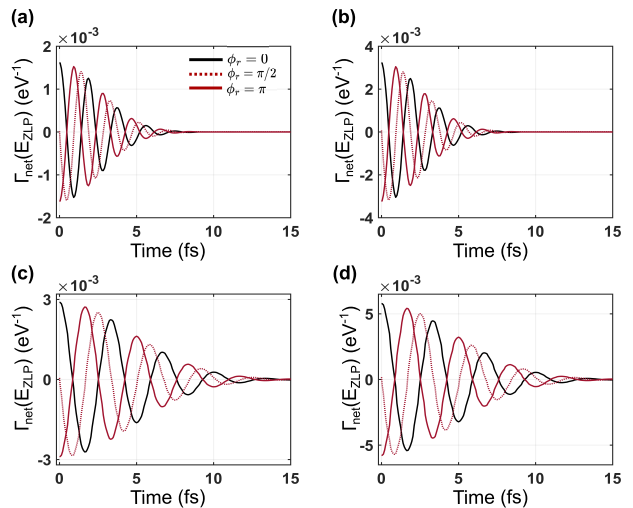


FIG. 3. (a)-(d) Dependence of the coherent oscillations in the zero-loss peak on the initial quantum coherence $(|g\rangle + e^{-i\phi_r}|e\rangle)/\sqrt{2}$. The relative phase effects shown for two impact parameters (a),(c) $r_\perp = 2\text{nm}$ and (b),(d) $r_\perp = 1\text{nm}$. The transition wavelengths used in (a),(b) and (c),(d) are the same as in Fig. 2(b) and Fig. 2(e), respectively.

The aim of coherent spectroscopic techniques is to probe the coherence of material excitations and to characterize their quantum-coherent dynamics. A major challenge is to coherently control and manipulate the quantum states of emitters in their local environment. Free electrons provide the high spatial resolution needed to access the coherence of individual quantum emitters prepared in superposition states. Beyond the probing of static off-diagonal density-matrix elements that requires preshaped electrons [10, 11], the time evolution of quantum superpositions can be tracked even with unmodulated electron wavepackets. This opens the way to novel transient spectroscopic techniques offering high spatial and temporal resolution for the study of dynamical processes in quantum systems.

We now discuss the experimental feasibility of observing the theoretical predictions. The transient features in the population dynamics occur on femtosecond timescales. To probe such ultrafast coherent processes in time-resolved CL, electron-driven photon sources (EDPHS) are suitable candidates [19]. Spectroscopic techniques based on EDPHS have already demonstrated the ability to probe single quantum emitters with femtosecond time resolution [17]. To observe the dynamical coherence effects in EELS, a key challenge would be the implementation of novel *in situ* measurements to track the evolution of the electron energy spectrum. Suitable model quantum systems can be 2D materials that host defect centers [22, 23]. Additionally, quantum dots such as InGaAs/GaAs act as ideal two-level emitters [24–27]. These materials exhibit dipole moments of the order of 20-40 debye [28] and transition frequencies in the IR region, which is within the range of parameters considered

here.

It is important to mention the validity of the theoretical framework. The coupling regime explored here is for weak interactions, $\text{Max}\{|g(z, t)|\} \ll 1$. For material systems with very large dipole moments such as perovskite nanocrystals [29, 30] and Rydberg atoms [31], there can be an enhanced electron-emitter coupling resulting in stronger coherence effects. The higher-order terms in the Magnus expansion could be important in such cases. In addition, impact parameters smaller than the size of the emitter may result in corrections to the dipole approximation.

To conclude, our analysis reveals the potential of free electrons to probe the coherence dynamics in quantum emitters. For initial superposition states, the populations exhibit transient oscillations that are sensitive to the relative phase. A crucial finding is the signature of quantum coherence of the emitter in the time-dependent

EELS spectra. Looking forward, generalizations to multilevel quantum systems [32], ensembles [14], and interactions with shaped electron wavefunctions [10, 33–35] would enable the study of the excited-state dynamics and entanglement evolution in quantum systems. The theoretical framework therefore lays the ground for related works. Finally, the ability to probe quantum-coherent dynamics with free electrons is attractive for exploring ultrafast coherent-state transfer in quantum spin chains with high spatial and temporal resolution.

This project has received funding from the Volkswagen Foundation (Momentum Grant) and from the European Research Council (ERC) under the European Union’s Horizon 2020 research and innovation programme, under grant agreement No. 101170341 (ERC Consolidator Grant UltraSpecT) and grant agreement No. 101017720 (EBEAM).

-
- [1] N. Talebi, *Near-Field-Mediated Photon–Electron Interactions* (Springer International Publishing, 2019); Interaction of electron beams with optical nanostructures and metamaterials: from coherent photon sources towards shaping the wave function, *J. Opt.* **19**, 103001 (2017).
- [2] A. Polman, M. Kociak, and F. J. García de Abajo, Electron-beam spectroscopy for nanophotonics, *Nat. Mater.* **18**, 1158 (2019).
- [3] F. Hayee, L. Yu, J. L. Zhang, C. J. Ciccarino, M. Nguyen, A. F. Marshall, I. Aharonovich, J. Vučković, P. Narang, T. F. Heinz, and J. A. Dionne, Revealing multiple classes of stable quantum emitters in hexagonal boron nitride with correlated optical and electron microscopy, *Nat. Mater.* **19**, 534 (2020).
- [4] F. J. García de Abajo and M. Kociak, Probing the photonic local density of states with electron energy loss spectroscopy, *Phys. Rev. Lett.* **100**, 106804 (2008).
- [5] A. J. Heinrich, W. D. Oliver, L. M. K. Vander-sypen, A. Ardavan, R. Sessoli, D. Loss, A. B. Jayich, J. Fernandez-Rossier, A. Laucht, and A. Morello, Quantum-coherent nanoscience, *Nat. Nanotechnol.* **16**, 1318 (2021).
- [6] I. Aharonovich, D. Englund, and M. Toth, Solid-state single-photon emitters, *Nat. Photonics* **10**, 631 (2016).
- [7] D. D. Awschalom, R. Hanson, J. Wrachtrup, and B. B. Zhou, Quantum technologies with optically interfaced solid-state spins, *Nat. Photonics* **12**, 516 (2018).
- [8] D. Loss and D. P. DiVincenzo, Quantum computation with quantum dots, *Phys. Rev. A* **57**, 120 (1998).
- [9] A. Gover and A. Yariv, Free-electron–bound-electron resonant interaction, *Phys. Rev. Lett.* **124**, 064801 (2020).
- [10] R. Ruimy, A. Gorlach, C. Mechel, N. Rivera, and I. Kaminer, Toward atomic-resolution quantum measurements with coherently shaped free electrons, *Phys. Rev. Lett.* **126**, 233403 (2021).
- [11] Z. Zhao, X.-Q. Sun, and S. Fan, Quantum entanglement and modulation enhancement of free-electron–bound-electron interaction, *Phys. Rev. Lett.* **126**, 233402 (2021).
- [12] B. Zhang, D. Ran, R. Ianculescu, A. Friedman, J. Scheuer, A. Yariv, and A. Gover, Quantum wave-particle duality in free-electron–bound-electron interaction, *Phys. Rev. Lett.* **126**, 244801 (2021).
- [13] B. Zhang, D. Ran, R. Ianculescu, A. Friedman, J. Scheuer, A. Yariv, and A. Gover, Quantum state interrogation using a preshaped free electron wavefunction, *Phys. Rev. Research* **4**, 033071 (2022).
- [14] R. Ruimy, A. Gorlach, G. Baranes, and I. Kaminer, Superradiant electron energy loss spectroscopy, *Nano Lett.* **23**, 779 (2023).
- [15] K. M. Roccapiore, R. Torsi, J. Robinson, S. Kalinin, and M. Ziatdinov, Dynamic stem-eels for single-atom and defect measurement during electron beam transformations, *Sci. Adv.* **10**, eadn5899 (2024).
- [16] W. Lee, L. D. Palmer, T. E. Gage, and S. K. Cushing, Imaging nanoscale carrier, thermal, and structural dynamics with time-resolved and ultrafast electron energy-loss spectroscopy, *Chem. Phys. Rev.* **6**, 041303 (2025).
- [17] M. Taleb, P. H. Bittorf, M. Black, M. Hentschel, W. Sigle, B. Haas, C. Koch, P. A. van Aken, H. Giessen, and N. Talebi, Ultrafast phonon-mediated dephasing of color centers in hexagonal boron nitride probed by electron beams, *Nat. Commun.* **16**, 2326 (2025).
- [18] D. Timmer, M. Gittinger, T. Quenzel, S. Stephan, Y. Zhang, M. F. Schumacher, A. Lützen, M. Silies, S. Tretiak, J.-H. Zhong, A. De Sio, and C. Lienau, Plasmon mediated coherent population oscillations in molecular aggregates, *Nat. Commun.* **14**, 8035 (2023).
- [19] M. Taleb, M. Hentschel, K. Rossnagel, H. Giessen, and N. Talebi, Phase-locked photon–electron interaction without a laser, *Nat. Phys.* **19**, 869 (2023).
- [20] R. P. Feynman, R. B. Leighton, and M. Sands, *The Feynman Lectures on Physics, Mainly Electromagnetism and Matter*, Vol. 2 (Addison-Wesley, Reading, 1964).
- [21] W. Magnus, On the exponential solution of differential equations for a linear operator, *Commun. Pure Appl. Math.* **7**, 649 (1954).
- [22] A. B. D. Shaik and P. Palla, Optical quantum technologies with hexagonal boron nitride single photon sources, *Sci. Rep.* **11**, 12285 (2021).
- [23] S. I. Azzam, K. Parto, and G. Moody, Prospects and

- challenges of quantum emitters in 2d materials, *Appl. Phys. Lett.* **118**, 240502 (2021).
- [24] H. Kamada, H. Gotoh, J. Temmyo, T. Takagahara, and H. Ando, Exciton rabi oscillation in a single quantum dot, *Phys. Rev. Lett.* **87**, 246401 (2001).
- [25] T. H. Stievater, X. Li, D. G. Steel, D. Gammon, D. S. Katzer, D. Park, C. Piermarocchi, and L. J. Sham, Rabi oscillations of excitons in single quantum dots, *Phys. Rev. Lett.* **87**, 133603 (2001).
- [26] B. Patton, U. Woggon, and W. Langbein, Coherent control and polarization readout of individual excitonic states, *Phys. Rev. Lett.* **95**, 266401 (2005).
- [27] X. Xu, B. Sun, P. R. Berman, D. G. Steel, A. S. Bracker, D. Gammon, and L. J. Sham, Coherent optical spectroscopy of a strongly driven quantum dot, *Science* **317**, 929 (2007).
- [28] K. L. Silverman, R. P. Mirin, S. T. Cundiff, and A. G. Norman, Direct measurement of polarization resolved transition dipole moment in ingaas/gaas quantum dots, *Appl. Phys. Lett.* **82**, 4552 (2003).
- [29] B. R. Sutherland and E. H. Sargent, Perovskite photonic sources, *Nat. Photonics* **10**, 295 (2016).
- [30] A. K. Jena, A. Kulkarni, and T. Miyasaka, Halide perovskite photovoltaics: Background, status, and future prospects, *Chem. Rev.* **119**, 3036 (2019).
- [31] R. G. Hulet, E. S. Hilfer, and D. Kleppner, Inhibited spontaneous emission by a rydberg atom, *Phys. Rev. Lett.* **55**, 2137 (1985).
- [32] H. B. Crispin and N. Talebi, Electron-beam-induced quantum interference effects in a multilevel quantum emitter, *Phys. Rev. B* **112**, 045419 (2025).
- [33] N. Talebi, Strong interaction of slow electrons with near-field light visited from first principles, *Phys. Rev. Lett.* **125**, 080401 (2020).
- [34] F. Chahshouri and N. Talebi, Tailoring near-field-mediated photon electron interactions with light polarization, *New J. Phys.* **25**, 013033 (2023).
- [35] F. Chahshouri and N. Talebi, Ultrafast plasmonic rotors for electron beams, *Nanophotonics* **14**, 2199 (2025).

**SUPPLEMENTARY MATERIAL: PROBING QUANTUM-COHERENT DYNAMICS WITH FREE
ELECTRONS**

S1. Time-dependent quantum theory for the coherent interaction between a free electron and a quantum emitter

In this section, we present a formulation of the theory describing the quantum-coherent dynamics in the populations and EELS. We start from the Hamiltonian that governs the coupling of the two-level emitter to the evanescent electric field of the propagating electron,

$$H = \frac{\hbar\omega_0}{2}\sigma_z - i\hbar v_0\partial_z + (\mathbf{d}_{eg}S^+ + \mathbf{d}_{eg}^*S^-) \cdot \vec{E}(r_\perp, 0, z). \quad (10)$$

This model Hamiltonian has been extensively discussed in the context of coherently modulated electron wavepackets [1, 2, 3, 4, 5] and its derivation can be found in Ref. [2]. To probe the ultrafast quantum dynamics, we must consider the time-dependent evolution of the joint free-electron and emitter. This is relevant for quantum emitters in emerging two-dimensional material systems and essential for understanding the coherent interactions in recent time-resolved CL measurements [6]. As mentioned in the main text, we use the interaction picture $H_I(t) = U(H - H_0)U^\dagger$ with respect to the unitary transformation $U = \exp\{iH_0t/\hbar\}$, where $H_0 = \hbar\omega_0\sigma_z/2 - i\hbar v_0\partial_z$. The solution can be written as

$$|\psi(t)\rangle = e^{\sum_k \Omega_k(t)} |\psi(t_0)\rangle, \quad (11)$$

where $|\psi(t_0)\rangle = |\psi_{qe}\rangle |\psi_{el}\rangle$ is the initial state of the free electron and the emitter in the interaction picture and Ω_k are the terms in the Magnus expansion. We describe the free electron by a Gaussian wavepacket in the position basis,

$$|\psi_{el}\rangle = \frac{1}{(2\pi\sigma_z^2)^{1/4}} \int dz e^{-\frac{z^2}{4\sigma_z^2} + ik_0z} |z\rangle. \quad (12)$$

Here, $k_0 = E_0v_0/\hbar c^2$ for an initial electron energy $E_0 = c\sqrt{m^2c^2 + \hbar^2k_0^2}$ with spatial width σ_z . The state (12) is expressed in the interaction picture and constant shifts in the basis ($|z + 2v_0t_0\rangle \equiv |z\rangle$) can be ignored as they play no role in the time evolution of the observables considered here. We are primarily interested in quantum systems prepared in general superposition states. The initial state of the two-level emitter is thus given by

$$|\psi_{qe}\rangle = a|g\rangle + b e^{-i\phi_r} |e\rangle, \quad (13)$$

with $a^2 + b^2 = 1$ and $\phi_r = \phi - \omega_0t_0$ being the relative phase of the coherent superposition.

Since the interaction between the quantum emitter and the electron wavepacket is weak, the higher-order terms in the Magnus series can be neglected. We focus on the dynamics governed by the first term in the expansion, which reads

$$\Omega_1 = -\frac{i}{\hbar} \int_{t_0}^t H_I(t_1) dt_1, \quad (14)$$

where the interaction Hamiltonian $H_I(t)$ is given by

$$H_I(t) = (\mathbf{d}_{eg}S^+ e^{i\omega_0t} + \mathbf{d}_{eg}^*S^- e^{-i\omega_0t}) \cdot \vec{E}(r_\perp, 0, z + v_0t), \quad (15)$$

and the electric field $\vec{E}(r_\perp, 0, z)$ of the propagating electron has the form

$$\vec{E}(r_\perp, 0, z) = \frac{-e\gamma}{4\pi\epsilon_0} \frac{(z\hat{e}_z + r_\perp\hat{e}_x)}{(\gamma^2z^2 + r_\perp^2)^{3/2}}. \quad (16)$$

Substituting Eq. (15) in Eq. (14), we find

$$\Omega_1 = -i \int_{t_0}^t \left(\frac{1}{\hbar} [\mathbf{d}_{eg} \cdot \vec{E}(r_\perp, 0, z + v_0t_1)] S^+ e^{i\omega_0t_1} + \text{H.c.} \right) dt_1. \quad (17)$$

We now make a change of variables $s = z + v_0 t_1$ and $ds = v_0 dt_1$. The above integral can be written as

$$\Omega_1 = -i \left(\frac{1}{\hbar v_0} \left\{ e^{-i \frac{\omega_0}{v_0} z} \int_{z+v_0 t_0}^{z+v_0 t} ds [\mathbf{d}_{eg} \cdot \vec{E}(r_\perp, 0, s)] e^{i \frac{\omega_0}{v_0} s} \right\} S^+ + \text{H.c.} \right). \quad (18)$$

We note that the relevant distance for the interaction would be a very small region, typically hundreds of nanometers around the location of the quantum emitter at the origin. In comparison, the electron traverses a much greater distance (on the order of hundreds of micrometers) from its source to the emitter's position, which allows us to extend the lower limit of the integral (18) to $-\infty$. Therefore, we have the following expression

$$\Omega_1 = -i \left(\frac{1}{\hbar v_0} \left\{ e^{-i \frac{\omega_0}{v_0} z} \int_{-\infty}^{z+v_0 t} ds [\mathbf{d}_{eg} \cdot \vec{E}(r_\perp, 0, s)] e^{i \frac{\omega_0}{v_0} s} \right\} S^+ + \text{H.c.} \right). \quad (19)$$

In a more compact form, we can write Eq. (19) as

$$\Omega_1 = -i [g(z, t) S^+ + \text{H.c.}], \quad (20)$$

where the *time-dependent* coupling parameter reads

$$g(z, t) = e^{-i \frac{\omega_0}{v_0} z} \left\{ \eta \int_{-\infty}^{z+v_0 t} ds \left[\frac{s \mathbf{d}_z + r_\perp \mathbf{d}_x}{(\gamma^2 s^2 + r_\perp^2)^{3/2}} \right] e^{i \frac{\omega_0}{v_0} s} \right\}. \quad (21)$$

In arriving at Eq. (21), we have made use of the electric field (16), expressed the transition dipole moment in terms of its components $\mathbf{d}_{eg} = \mathbf{d}_x \hat{e}_x + \mathbf{d}_y \hat{e}_y + \mathbf{d}_z \hat{e}_z$, and set $\eta = -e\gamma/4\pi\epsilon_0 \hbar v_0$.

To proceed further, we employ the Leibniz rule to differentiate under the integral sign. Using this method, it can be shown that an integral $\mathcal{I}(\alpha) = \int_{-\infty}^{\tilde{z}} ds e^{i\alpha s} (\gamma^2 s^2 + r_\perp^2)^{-3/2}$ satisfies a nonhomogenous Bessel differential equation of the form $\mathcal{I}''(\alpha) - \alpha^{-1} \mathcal{I}'(\alpha) - \frac{r_\perp^2}{\gamma^2} \mathcal{I}(\alpha) = f(\alpha)$, where $\mathcal{I}'(\alpha) \equiv d\mathcal{I}/d\alpha$ and $\mathcal{I}''(\alpha) \equiv d^2\mathcal{I}/d\alpha^2$ are the first and second-order derivatives with respect to the parameter α . It is then straightforward to find the solution $\mathcal{I}(\alpha)$ to this differential equation using standard techniques. We present here the final result, which is the exact semi-analytical solution for the time-dependent coupling parameter (21), expressed as

$$g(z, t) = e^{-i \frac{\omega_0}{v_0} z} [g_0(z, t) + g_1(z, t)], \quad (22)$$

with

$$g_0 = \frac{\eta \omega_0}{\gamma^2 v_0} \left\{ \mathbf{d}_x K_1 \left(\frac{r_\perp \omega_0}{\gamma v_0} \right) + \frac{i \mathbf{d}_z}{\gamma} K_0 \left(\frac{r_\perp \omega_0}{\gamma v_0} \right) \right\} \left[1 + \frac{\gamma(z + v_0 t)}{\sqrt{\gamma^2(z + v_0 t)^2 + r_\perp^2}} \right], \quad (23)$$

$$g_1 = \frac{\eta r_\perp \omega_0}{\gamma^2 v_0 \sqrt{\gamma^2(z + v_0 t)^2 + r_\perp^2}} \left[g_K \int_0^{\frac{\omega_0}{v_0}} ds \frac{e^{is(z+v_0 t)}}{s} I_1 \left(\frac{r_\perp s}{\gamma} \right) - g_I \int_{\frac{\omega_0}{v_0}}^\infty ds \frac{e^{is(z+v_0 t)}}{s} K_1 \left(\frac{r_\perp s}{\gamma} \right) \right],$$

The constant coefficients g_i ($i = K, I$) read $g_I = [i \mathbf{d}_x I_1(r_\perp \omega_0 / \gamma v_0) + \mathbf{d}_z I_0(r_\perp \omega_0 / \gamma v_0)] / \gamma$ and $g_K = [i \mathbf{d}_x K_1(r_\perp \omega_0 / \gamma v_0) + \mathbf{d}_z K_0(r_\perp \omega_0 / \gamma v_0)] / \gamma$, where $I_v(x)$ and $K_v(x)$ are the modified Bessel functions of the first and second kind, respectively. It is easy to see that in the long-time limit $t \rightarrow \infty$, $g_1 \rightarrow 0$ and $g_0(z, t)$ reduces to

$$\lim_{t \rightarrow \infty} g_0(z, t) \equiv g_\infty = \frac{2\eta \omega_0}{\gamma^2 v_0} \left\{ \mathbf{d}_x K_1 \left(\frac{r_\perp \omega_0}{\gamma v_0} \right) + \frac{i \mathbf{d}_z}{\gamma} K_0 \left(\frac{r_\perp \omega_0}{\gamma v_0} \right) \right\}, \quad (24)$$

which is the standard coupling constant that arises in a full scattering matrix description of a free electron interacting with a two-level system [2,3]. Interestingly, the parameters $g_i(z, t)$ ($i = 0, 1$) depend on the variables z and t as $\tilde{z} = z + v_0 t$. Taking advantage of this fact, it is useful to go to the spectral domain via the transforms:

$$g(\tilde{z}) = \int d\omega \tilde{g}(\omega) e^{-i \frac{\omega}{v_0} \tilde{z}} \quad \tilde{g}(\omega) = \frac{1}{2\pi v_0} \int d\tilde{z} g(\tilde{z}) e^{i \frac{\omega}{v_0} \tilde{z}}, \quad (25)$$

where the time-dependence is implicit in $\tilde{z} = z + v_0 t$. Using these relations, the dynamical coupling $\tilde{g}(\omega)$ is given by

$$\tilde{g}(\omega) = [\delta(\omega - \omega_0) g_q(\omega_0) + g_c(\omega)] e^{i \omega_0 t}. \quad (26)$$

The above expression has a clear physical interpretation in the context of the electron momentum ladder operators

$$b(\omega) = e^{-i\frac{\omega}{v_0}z}, \quad b^\dagger(\omega) = e^{i\frac{\omega}{v_0}z}, \quad (27)$$

where $b(\omega)$ [$b^\dagger(\omega)$] lowers [raises] the electron momentum by $\hbar\omega/v_0$. We now see that the parameter $g(\tilde{z}) = \int d\omega \tilde{g}(\omega) b(\omega) e^{-i\omega t}$ can be viewed as the electron ladder operator weighted by $\tilde{g}(\omega)$. The Dirac delta δ is therefore responsible for the free electron gaining or losing exactly the energy $\hbar\omega_0$ of the two-level transition with a constant coefficient $g_q(\omega_0) = g_\infty/2$. In contrast, the spectral weight $g_c(\omega)$ evolves as $e^{-i(\omega-\omega_0)t}$ and leads to changes in the electron energy that is detuned from the transition energy $\hbar\omega_0$. The explicit form of $g_c(\omega)$ is given in Appendix A. In Secs. **S2** and **S3**, we make use of the solutions (22) and (26) to understand the qualitative features in the population dynamics and the EELS spectra.

Finally, with the dynamics governed only by Ω_1 (20), it is straightforward to express the solution (11) in the position basis $\int dz |z\rangle \langle z|$ and write the joint quantum state of the electron wavepacket and the two-level emitter as

$$|\psi(t)\rangle = \int dz e^{-\frac{z^2}{4\sigma_z^2} + ik_0 z} [c_g(z, t) |g\rangle + c_e(z, t) |e\rangle] |z\rangle, \quad (28)$$

where the initial states of the quantum emitter and the free electron are according to Eqs. (12) and (13). The probability amplitudes are found to be

$$\begin{aligned} c_g(z, t) &= [a \cos |g(z, t)| - i b e^{-i(\phi_r + \phi_g(z, t))} \sin |g(z, t)|], \\ c_e(z, t) &= [b e^{-i\phi_r} \cos |g(z, t)| - i a e^{i\phi_g(z, t)} \sin |g(z, t)|]. \end{aligned} \quad (29)$$

S2. Population dynamics

In this section, we derive a semianalytical form for the populations in the case of general superposition states of the quantum emitter. The qualitative features of our results can be easily understood with the help of these solutions. To investigate the quantum dynamics of the two-level emitter, we compute the reduced density matrix

$$\rho_{qe}(t) = \text{Tr}_{el}\{|\psi(t)\rangle \langle \psi(t)|\} = \frac{1}{\sqrt{2\pi\sigma_z}} \int dz e^{-\frac{z^2}{2\sigma_z^2}} \begin{pmatrix} |c_g(z, t)|^2 & c_g(z, t) c_e^*(z, t) \\ c_e(z, t) c_g^*(z, t) & |c_e(z, t)|^2 \end{pmatrix}, \quad (30)$$

where the diagonal elements $|c_g|^2$ and $|c_e|^2$ give the populations of the ground and excited states, respectively. Under the weak coupling assumption $|g(z, t)| \ll 1$, we can write the inversion $\rho_{ee} - \rho_{gg}$ approximately as

$$\rho_{ee} - \rho_{gg} = \frac{1}{\sqrt{2\pi\sigma_z}} \int dz e^{-\frac{z^2}{2\sigma_z^2}} [b^2 - a^2 + 4ab \text{Im}\{g(z, t) e^{i\phi_r}\}], \quad (31)$$

whereas the trace $\rho_{ee} + \rho_{gg}$ of the density matrix (30) naturally satisfies

$$\rho_{ee} + \rho_{gg} = \frac{1}{\sqrt{2\pi\sigma_z}} \int dz e^{-\frac{z^2}{2\sigma_z^2}} (a^2 + b^2) = 1. \quad (32)$$

The expression (31) can be further simplified to yield

$$\rho_{ee} - \rho_{gg} = b^2 - a^2 + 2ab e^{-\frac{\sigma_z^2 \omega_0^2}{2v_0^2}} \text{Im}\{g_\infty e^{i\phi_r}\} + 4ab \text{Im}\left\{ \int d\omega g_c(\omega) e^{-\frac{\sigma_z^2 \omega^2}{2v_0^2}} e^{-i(\omega-\omega_0)t + i\phi_r} \right\}, \quad (33)$$

where we have made use of Eqs. (24) and (25). We can therefore write the equations for the excited and ground state populations as

$$\begin{aligned} \rho_{ee} &= b^2 + ab e^{-\frac{\sigma_z^2 \omega_0^2}{2v_0^2}} \text{Im}\{g_\infty e^{i\phi_r}\} + 2ab \text{Im}\left\{ \int d\omega g_c(\omega) e^{-\frac{\sigma_z^2 \omega^2}{2v_0^2}} e^{-i(\omega-\omega_0)t + i\phi_r} \right\}, \\ \rho_{gg} &= a^2 - ab e^{-\frac{\sigma_z^2 \omega_0^2}{2v_0^2}} \text{Im}\{g_\infty e^{i\phi_r}\} - 2ab \text{Im}\left\{ \int d\omega g_c(\omega) e^{-\frac{\sigma_z^2 \omega^2}{2v_0^2}} e^{-i(\omega-\omega_0)t + i\phi_r} \right\}. \end{aligned} \quad (34)$$

It is obvious that the dynamics is entirely governed by the spectral coupling parameter $g_c(\omega)$. In addition, we can clearly see why the coherent oscillations cannot occur for an initial ground ($a = 1, b = 0$) or excited state ($a = 0,$

$b = 1$) of the two-level emitter. In such cases, the approximate expressions (34) show that the populations are nearly unchanged for weak interactions. However, for an initial superposition state, interesting coherence effects are induced by the electron wavepacket. A numerical analysis reveals that $g_c(\omega)$ is dominant around $\omega = \omega_0$ whereas the Gaussian prefactor $e^{-\sigma_z^2 \omega^2 / (2v_0^2)}$ has the maximum weight near $\omega = 0$. Therefore, heuristically considering $g_c(\omega) \approx g_c(\omega = 0)$ and pulling the spectral weight outside the integral, we see that the populations behave according to

$$\begin{aligned}\rho_{ee} &\sim b^2 + ab e^{-\frac{\sigma_z^2 \omega_0^2}{2v_0^2}} \text{Im}\{g_\infty e^{i\phi_r}\} + 4\sqrt{\pi} ab \frac{e^{-\frac{t^2}{\sigma_t^2}}}{\sigma_t} \text{Im}\{g_c(0)e^{i(\omega_0 t + \phi_r)}\}, \\ \rho_{gg} &\sim a^2 - ab e^{-\frac{\sigma_z^2 \omega_0^2}{2v_0^2}} \text{Im}\{g_\infty e^{i\phi_r}\} - 4\sqrt{\pi} ab \frac{e^{-\frac{t^2}{\sigma_t^2}}}{\sigma_t} \text{Im}\{g_c(0)e^{i(\omega_0 t + \phi_r)}\},\end{aligned}\quad (35)$$

where $\sigma_t = \sigma_z/v_0$ is the duration of the wavepacket. The coherent oscillations therefore arise from the exponential oscillatory term $e^{i\omega_0 t}$ with a temporal Gaussian envelope $e^{-t^2/(\sigma_t^2)}$. Thus, we have qualitatively shown the origin of the induced coherence effects in the populations.

S3. Quantum coherence effects in the EELS spectra

In this section, we discuss the electron energy spectra and show how the coherent features arise in the zero-loss peak of the spectral probability density. Let us consider the probability difference,

$$\Gamma_{net}(E, t) = \frac{1}{\hbar v_0} (|\psi_e(k(E), t)|^2 - |\psi_g(k(E), t)|^2), \quad (36)$$

where

$$\psi_i(k(E), t) = \frac{1}{N} \int dz e^{-z^2/4\sigma_z^2} e^{-ikz} c_i(z, t). \quad (37)$$

In this expression, $N = \sqrt{2\pi} (2\pi\sigma_z)^{1/4}$ is a multiplicative factor, $k(E) = (E - E_0)/\hbar v_0$, and $c_i(z, t)$ ($i = g, e$) are given by Eq. (29). In the regime of weak interactions $g(z, t) \ll 1$, we can write Eq. (37) as

$$\begin{aligned}\psi_e &= \frac{1}{N} \int dz e^{-z^2/4\sigma_z^2} e^{-ikz} [a - ib e^{-i\phi_r} g^*(z, t)], \\ \psi_g &= \frac{1}{N} \int dz e^{-z^2/4\sigma_z^2} e^{-ikz} [b e^{-i\phi_r} - ia g(z, t)].\end{aligned}\quad (38)$$

For brevity, we adopt the short-hand notation $\psi_i \equiv \psi_i(k(E), t)$ ($i = g, e$). We now proceed in a manner similar to that in the previous analysis. Using Eq. (25), the amplitudes ψ_i can be expressed as

$$\begin{aligned}\psi_e &= \frac{2\sqrt{\pi}\sigma_z}{N} [b e^{-i\phi_r} e^{-k^2\sigma_z^2} - ia \int d\omega \tilde{g}(\omega) e^{-i\omega t} e^{-\sigma_t^2 v_0^2 (k + \frac{\omega}{v_0})^2}], \\ \psi_g &= \frac{2\sqrt{\pi}\sigma_z}{N} [a e^{-k^2\sigma_z^2} - ib e^{-i\phi_r} \int d\omega \tilde{g}^*(\omega) e^{i\omega t} e^{-\sigma_t^2 v_0^2 (k - \frac{\omega}{v_0})^2}],\end{aligned}\quad (39)$$

where $\tilde{g}^*(\omega) = [\tilde{g}(\omega)]^*$ denotes the complex conjugate. It is clear that the second term gives rise to the sidebands in the EELS spectra with the Dirac delta $\delta(\omega - \omega_0)$ (26) leading to electron energy gain or loss of $\hbar\omega_0$ whereas the interesting oscillatory features originate from the spectral weight $g_c(\omega)$. To simplify the calculations, we consider an equally weighted superposition $a = b$, as in the main text. Since we are interested in the zero-loss peak, we set $k(E) = (E - E_0)/\hbar v_0 = 0$ in the above expression and assume that $g_c(\omega) \approx g_c(\omega = 0)$ since the Gaussian prefactor is centered at $\omega = 0$, which is far from the resonance of $g_c(\omega = \omega_0)$. Therefore, the time evolution of the amplitudes behaves according to

$$\begin{aligned}\psi_e &\sim \frac{2\sqrt{\pi}av_0}{N} [e^{-i\phi_r} \sigma_t - i \sigma_t g_q(\omega_0) e^{-\sigma_t^2 \omega_0^2} - i \sqrt{\pi} g_c(0) e^{i\omega_0 t} e^{-\frac{t^2}{4\sigma_t^2}}], \\ \psi_g &\sim \frac{2\sqrt{\pi}av_0}{N} [\sigma_t - i e^{-i\phi_r} \sigma_t g_q^*(\omega_0) e^{-\sigma_t^2 \omega_0^2} - i \sqrt{\pi} g_c^*(0) e^{-i(\omega_0 t + \phi_r)} e^{-\frac{t^2}{4\sigma_t^2}}].\end{aligned}\quad (40)$$

Using these relations, we find the probability difference $\Gamma_{net}(E, t)$ to be

$$\Gamma_{net}(E, t) \sim \frac{1}{\hbar v_0} \left(\frac{4\sqrt{\pi} a \sigma_z}{N} \right)^2 \left[\frac{1}{2} e^{-\sigma_t^2 \omega_0^2} \text{Im}\{g_\infty e^{i\phi_r}\} + \sqrt{\pi} \frac{e^{-\frac{t^2}{4\sigma_t^2}}}{\sigma_t} \text{Im}\{g_c(0) e^{i(\omega_0 t + \phi_r)}\} \right]. \quad (41)$$

This expression is identical to the equations (35) describing the behaviour of the populations. We find that the zero-loss peak coherently oscillates at the transition frequency ω_0 of the two-level emitter with a broad Gaussian envelope $e^{-t^2/(4\sigma_t^2)}$. Thus, a signature of the quantum coherence of the emitter is found in the EELS dynamics even for unmodulated electron wavepackets.

Appendix A

The expression for the spectral coupling parameter $g_c(\omega)$ that governs the population dynamics and the evolution of the electron energy spectrum is given by

$$\begin{aligned} g_c(\omega) = & \frac{1}{2\pi v_0} \left(g_\infty \left[\frac{ir_\perp}{\gamma} K_1 \left(\frac{r_\perp |\omega - \omega_0|}{\gamma v_0} \right) \text{sgn}(\omega - \omega_0) \right] \right. \\ & + \frac{2\eta r_\perp \omega_0}{\gamma^3 v_0} \left[g_K \int_0^{\frac{\omega_0}{v_0}} ds \frac{1}{s} I_1 \left(\frac{r_\perp s}{\gamma} \right) K_0 \left(\frac{r_\perp |sv_0 + \omega - \omega_0|}{\gamma} \right) \right. \\ & \left. \left. - g_I \int_{\frac{\omega_0}{v_0}}^\infty ds \frac{1}{s} K_1 \left(\frac{r_\perp s}{\gamma} \right) K_0 \left(\frac{r_\perp |sv_0 + \omega - \omega_0|}{\gamma} \right) \right] \right), \end{aligned} \quad (42)$$

where

$$\text{sgn}(\omega - \omega_0) = \begin{cases} +1, & \omega > \omega_0, \\ 0, & \omega = \omega_0, \\ -1, & \omega < \omega_0. \end{cases}$$

REFERENCES

- [1] A. Gover and A. Yariv, "Free-electron-bound-electron resonant interaction", *Phys. Rev. Lett.* **124**, 064801 (2020).
- [2] R. Ruimy, A. Gorchach, C. Mechel, N. Rivera, and I. Kaminer, "Toward atomic-resolution quantum measurements with coherently shaped free electrons", *Phys. Rev. Lett.* **126**, 233403 (2021).
- [3] Z. Zhao, X.-Q. Sun, and S. Fan, "Quantum entanglement and modulation enhancement of free-electron-bound electron interaction", *Phys. Rev. Lett.* **126**, 233402 (2021).
- [4] B. Zhang, D. Ran, R. Iancu, A. Friedman, J. Scheuer, A. Yariv, and A. Gover, "Quantum wave-particle duality in free-electron-bound-electron interaction", *Phys. Rev. Lett.* **126**, 244801 (2021).
- [5] B. Zhang, D. Ran, R. Iancu, A. Friedman, J. Scheuer, A. Yariv, and A. Gover, "Quantum state interrogation using a preshaped free electron wavefunction", *Phys. Rev. Research* **4**, 033071 (2022).
- [6] M. Taleb, P. H. Bittorf, M. Black, M. Hentschel, W. Sigle, B. Haas, C. Koch, P. A. van Aken, H. Giessen, and N. Talebi, "Ultrafast phonon-mediated dephasing of color centers in hexagonal boron nitride probed by electron beams", *Nat. Commun.* **16**, 2326 (2025).